Supporting Information

Asymmetric Carrier Transport in Flexible Interface-type Memristor Enables Artificial Synapses with Sub-Femtojoule Energy Consumption

June-Mo Yang, Young-Kwang Jung, Ju-Hee Lee, Yong Churl Kim, So-Yeon Kim, Seunghwan Seo, Dong-Am Park, Jeong-Hyeon Kim, Se-Yong Jeong, Jin-Hong Park, In-Taek Han, Aron Walsh, and Nam-Gyu Park

Experimental Methods

Materials. Cesium iodide (CsI) (99.9%, Alfa Aesar), copper (I) iodide (CuI) (99.5 %, Sigma Aldrich), PEDOT:PSS (Al 4083, Heraeus), dimethyl sulfoxide (DMSO) (≥99.9% anhydrous, Sigma Aldrich) and diethyl ether (99.7% anhydrous, Sigma Aldrich) were purchased and used without further purification.

Fabrication of synaptic devices. ITO-coated PET and glass substrates were ultrasonically cleaned with detergent, ethanol, acetone and ethanol, and was further treated by UV ozone for 60 min before spin-coating the PEDOT:PSS and $Cs_3Cu_2I_5$ films. PEDOT:PSS solution was deposited on ITO-coated substrates by spin-coating method at 4000 rpm for 20s (acceleration = 1200/rpm), which was followed by annealing at 150 ^oC for 15 min. $Cs_3Cu_2I_5$ precursor solution was prepared by dissolving 0.5 mmol of CsI (0.130 g) and 0.33mmol of CuI (0.0635 g) in 0.25 ml, 0.3 ml, 0.35 ml and 0.4 ml of DMSO for producing 340 nm-, 290 nm-, 240 nm- and 190 nm-thick $Cs_3Cu_2I_5$ films. Precursor solution was spin-coated on the PEDOT:PSS-coated substrate at 4000 rpm (acceleration = 1200/rpm) for 30 s, where diethyl ether was dropped while spin-coating (10s after spinning), which was annealed at 100 ^oC for 10min. 200

nm-thick Au top electrode was thermally evaporated on the $Cs_3Cu_2I_5$ film under 1.0×10^{-6} torr, where a shadow mask with holes of diameters of 50, 100, 200 and 400 μm was used.

Characterization. X-ray diffraction (XRD) patterns were measured by an X-ray diffractometer (Rigaku Smartlab SE) with Cu $K\alpha_1$ radiation (wavelength = 1.54056 Å). XRD data were collected in the 2θ range from 10° to 50° at scan speed of 2°/min with a step scan size of 0.01°. Surface and cross-sectional morphologies were investigated by using a field emission scanning electron microscope (FESEM) (JSM7401F, JEOL). Absorption and transmittance spectra were measured by using an UV–vis spectrometer (Lambda 45, Perkin Elmer). UPS was measured by using ESCALAB 250Xi (Theromo-Scientific). Capacitance was measured by impedance spectroscopy measurements (PGSTAT 128N, Autolab) with small perturbation of AC 20 mV and frequencies ranging from 100 mHz to 1 MHz in the dark. Thickness of $Cs_3Cu_2I_5$ films was measured by alpha-step IQ surface profiler (KLA Tencor). All electrical characteristics were measured with a vacuum probe station equipped with Keithley 4200 source meter under ca. 10^{-2} torr.

First-principles simulations. Calculations were performed starting from the experimental crystal structure of $Cs_3Cu_2I_5$. The fully optimized structural model was used to explore the electronic band structure and effective masses, and as the starting point for the point defect investigations. All calculations were performed based on Kohn-Sham DFT[1] where periodic boundary conditions are considered. The Vienna Ab Initio Simulation Package (VASP)[2,3] was used with Projector augmented-wave (PAW)[4,5] pseudo-potentials. The Perdew-Burke-Ernzerhof exchange-correlation functional revised for solids (PBEsol)[6] with the plane-wave kinetic energy cutoff of 700 eV was employed. 3×3×2 Γ-centered **k**-mesh and was adopted for optimizing primitive unit cell (40 atoms) of $Cs_3Cu_2I_5$ where convergence criteria were set to

10^{-5} eV and 10^{-2} eVÅ^{-1} for total energy and forces on each atoms, respectively. The electronic band structure was computed with Wannier interpolation of the HSE06[7,8] electronic structure using Wannier90 code.[9-11] For defect calculations, we modeled vacancy containing super cells where $\sqrt{2} \times \sqrt{2} \times 1$ super cell expansion was adopted. With fixed lattice constants, we fully relaxed internal atomic coordination under the same condition we used for the primitive cell optimization process. Only **k**-mesh was reduced to 2×2×2 grids. To study the vacancy mediated ion migration in $Cs_3Cu_2I_5$, we performed climbing-image NEB calculations[12] where the same super cell size, **k**-mesh grid and kinetic energy cutoff as the defect calculations. Only convergence criteria of forces during the NEB calculations was increased to 5×10^{-2} eVÅ^{-1}. We considered all possible vacancy site based on Wyckoff positions and sampled migration path based on inter atomic distance between distinct Cs-Cs, Cu-Cu, I-I pairs, respectively. All visualization of atomic structures was done using VESTA3 software.[13]

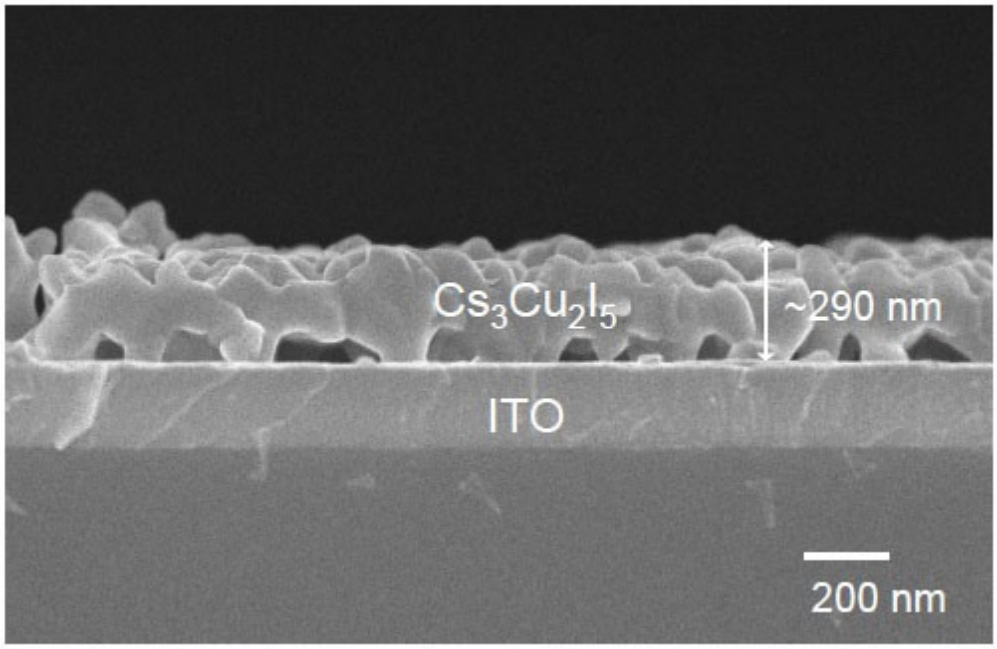

Figure S1. Cross-sectional SEM image of $Cs_3Cu_2I_5$ deposited on the PEDOT:PSS-coated ITO.

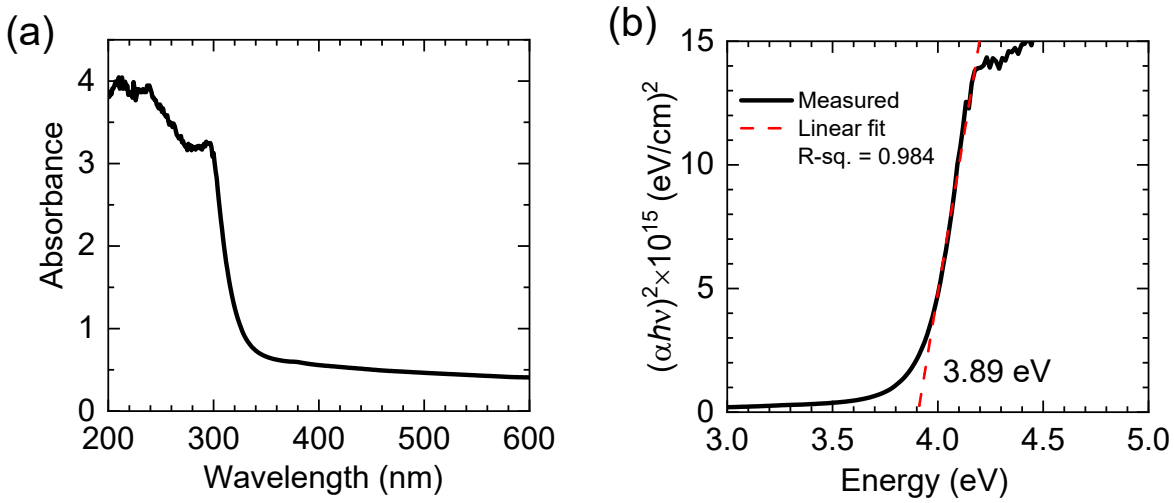

Figure S2. (a) Absorbance spectra and (b) Tauc plot of the $Cs_3Cu_2I_5$ film. Optical bandgap was determined by liner fit.

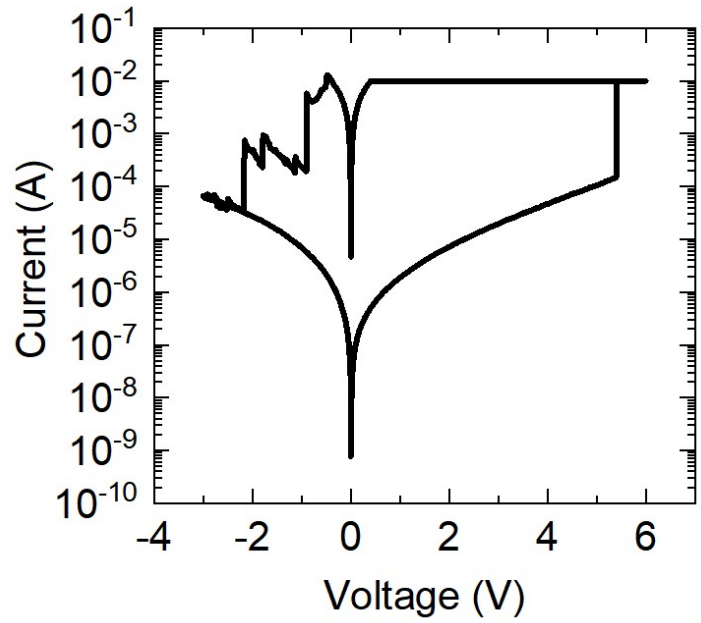

Figure S3. I-V curve of flexible $Cs_3Cu_2I_5$ memristor with bending radius of 5 mm.

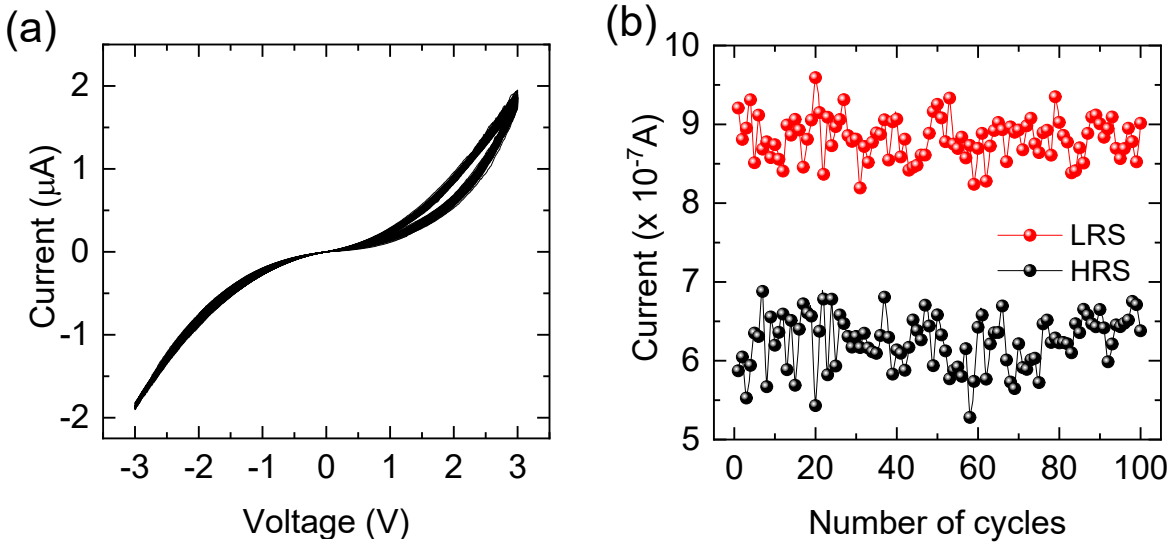

Figure S4. (a) I-V curves of the given single cell for 100 cycles. Voltage sweeps from 0 V, +3 V, 0 V, -3 V and 0 V were applied for 100 cycles. (b) Current of LRS and HRS at 2 V for 100 cycles.

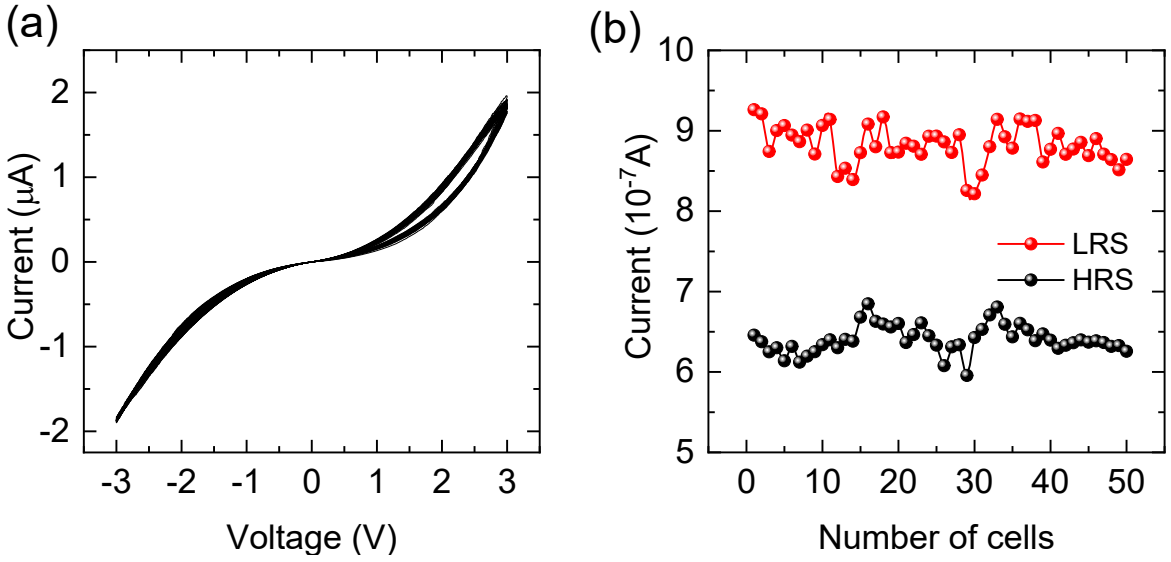

Figure S5. (a) I-V curves for 50 different cells in one mother device. Voltage sweeps from 0 V, +3 V, 0 V, -3 V and 0 V were applied. (b) Current of LRS and HRS at 2 V.

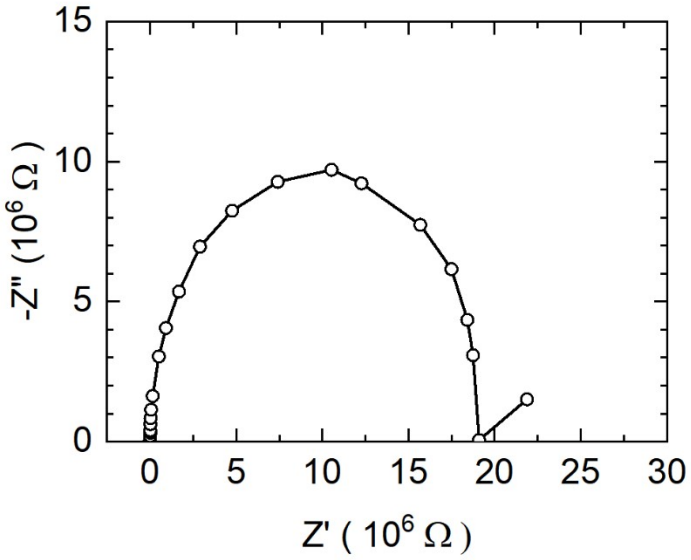

Figure S6. Nyquist plot for the capacitance-frequency data in Figure 2(c) in the manuscript.

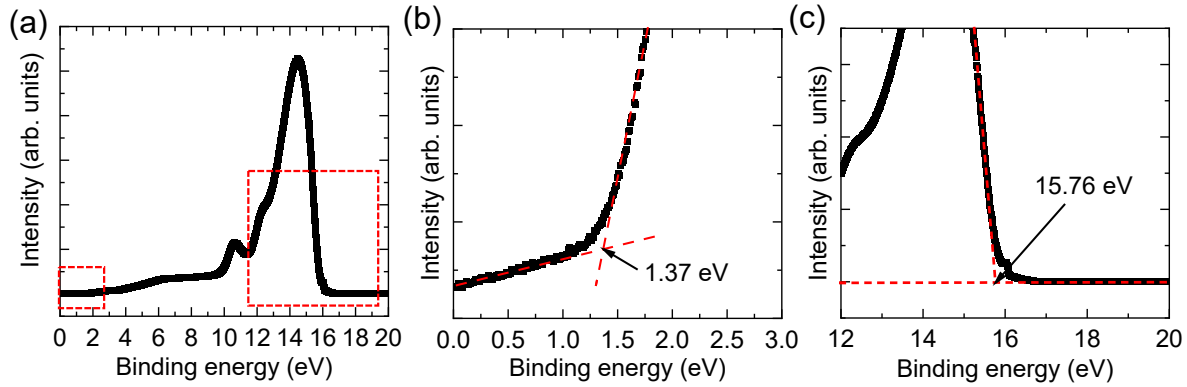

Figure S7. (a) Ultraviolet photoelectron spectroscopy (UPS) for $Cs_3Cu_2I_5$ films. (b) The binding energies of the valence band (E_{vb}) and (c) the cut-off ($E_{cut\text{-}off}$). Si substrates were used to measure UPS.

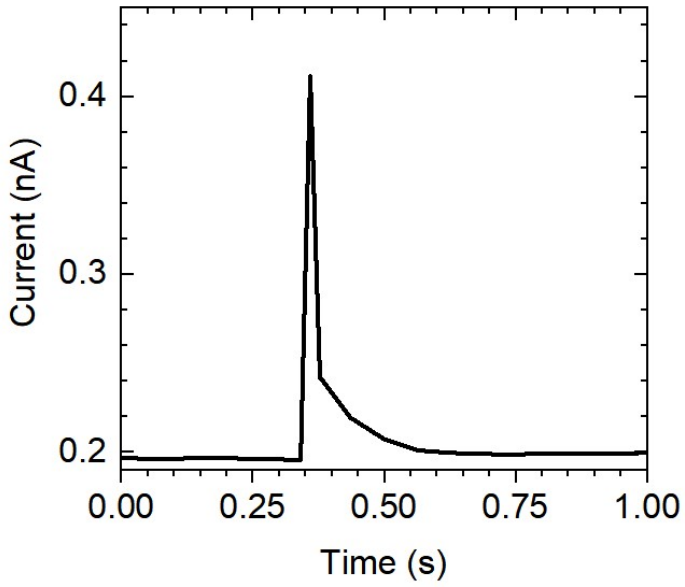

Figure S8. EPSC characteristics observed at a 500 μs pulse of 0.1 V with peak current.

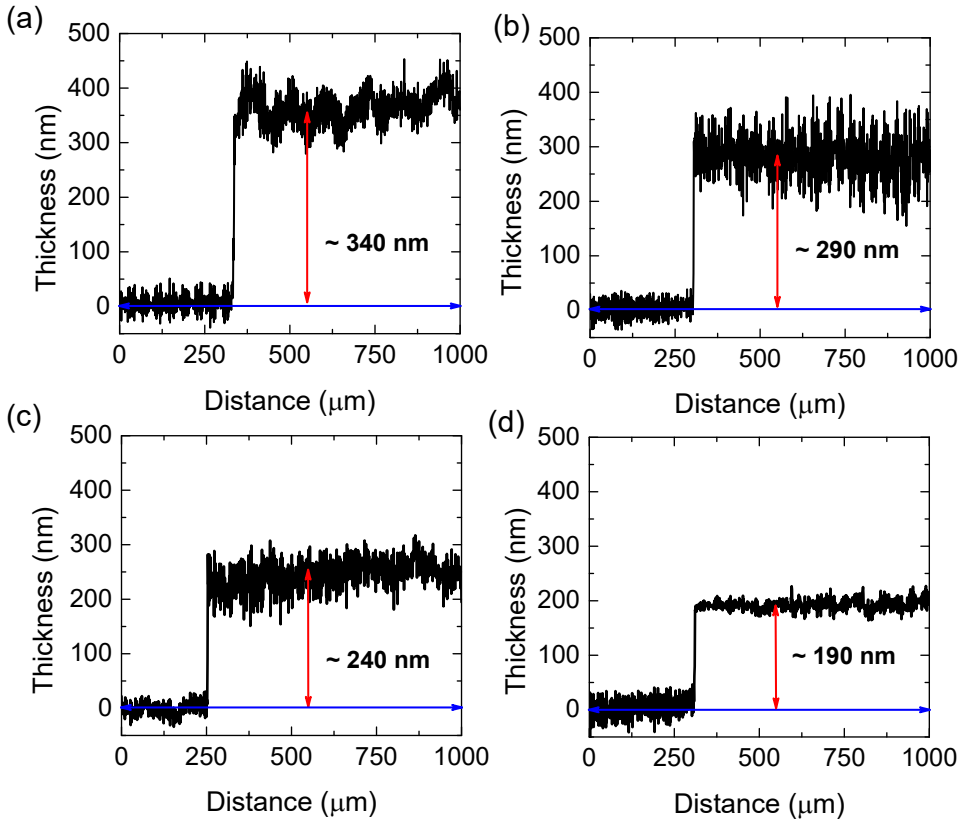

Figure S9. $Cs_3Cu_2I_5$ film thickness fabricated from the precursor solution with DMSO of (a) 0.25 ml, (b) 0.3 ml, (c) 0.35 ml and (d) 0.4 ml.

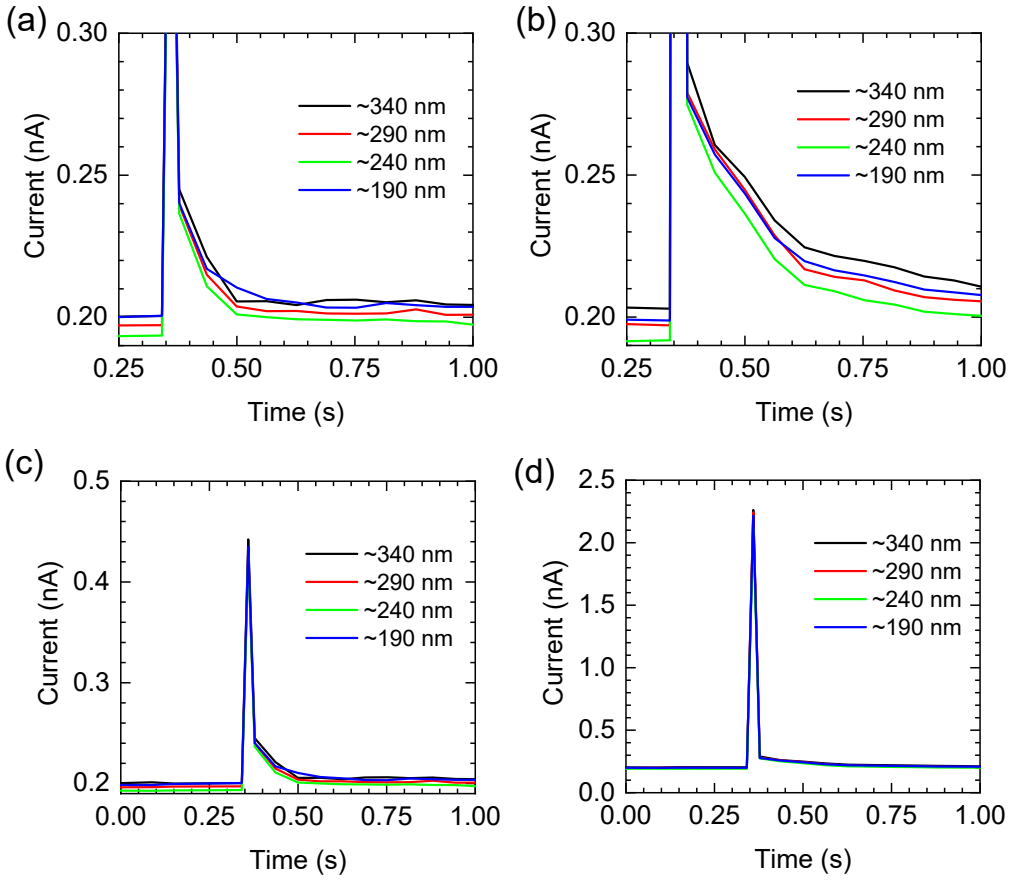

Figure S10. EPSC characteristics for the 340 nm-, 290 nm-, 240 nm- and 190 nm-thick $Cs_3Cu_2I_5$ films in flexbile devices observed at a 500 μs pulse of (a) 0.1 V and (b) 0.5 V. (c) and (d) shows peak current at a 500 μs pulse for 0.1 V and 0.5 V, respectively.

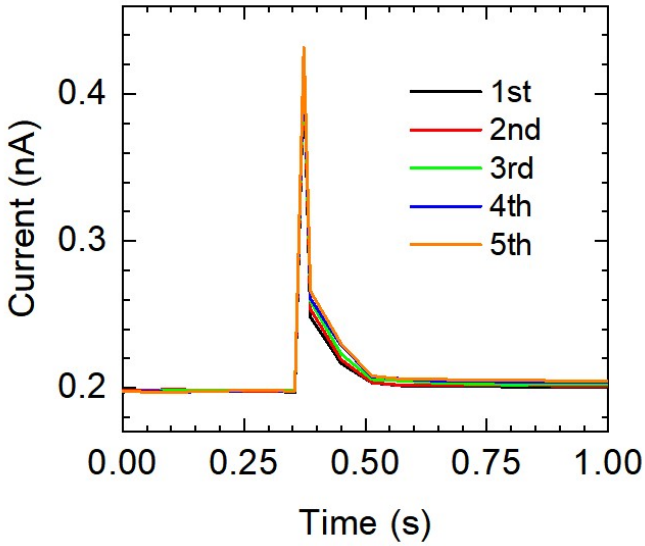

Figure S11. EPSC characteristics with peak current observed when 500 μs pulses of 0.1 V were applied 5 times for measurement of SNDP.

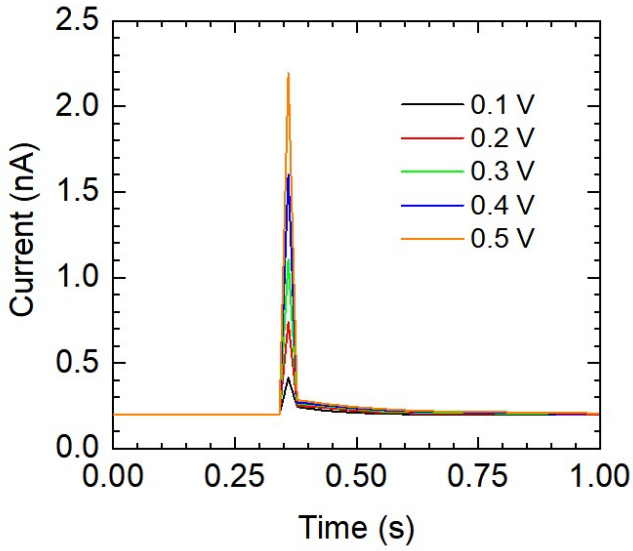

Figure S12. EPSC characteristics with peak current observed when 500 μs pulses of 0.1 V, 0.2 V, 0.3 V, 0.4 V and 0.5 V were applied for measurement of SVDP.

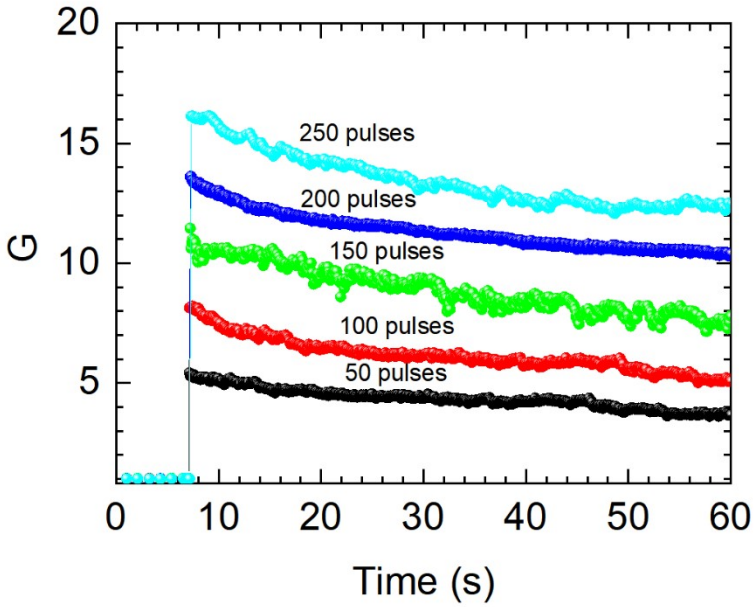

Figure S13. LTP depnding on the number of pulses.

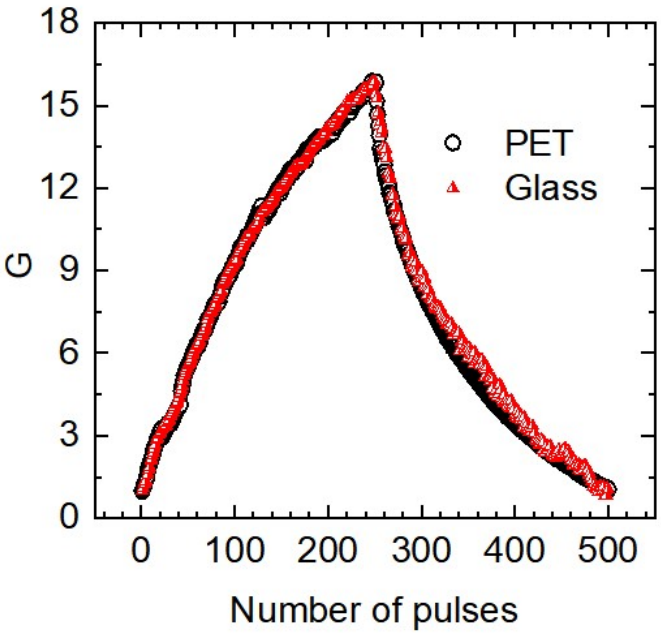

Figure S14. Comparison of potentiation and depression between glass substrate and flexible PET substrate, where 250 consecutive positive pulses (2.5 V, 700 μs) for potentiation were followed by 250 negative pulses (-1 V, 700 μs) for depression. 0.1 V reading voltage was applied after each positive and negative pulse.

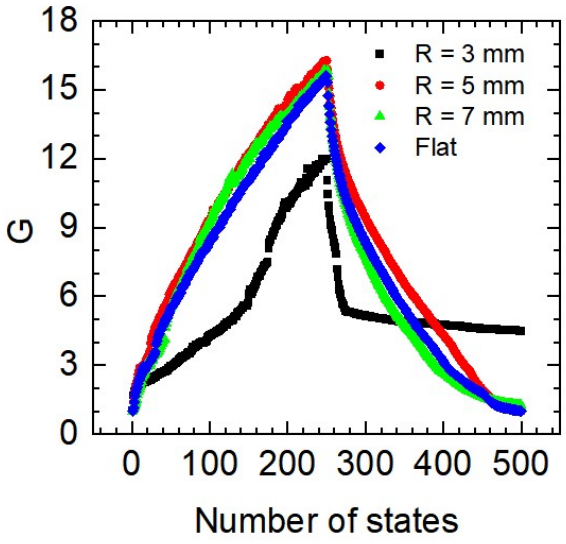

Figure S15. Potentiation and depression as a function of the number of pulses depending on bending radius (R), where 250 consecutive positive pulses (2.5 V, 700 μs) for potentiation were followed by 250 negative pulses (-1 V, 700 μs) for depression. 0.1 V reading voltage was applied after each positive and negative pulse.

References

[1] W. Kohn, L. J. Sham, *Phys. Rev*., 1965, **140**, A1133.

[2] G. Kresse, J. Furthmüller, *Phys. Rev. B*., 1996, **54**, 11169.

[3] G. Kresse, J. Furthmüller, *Comput. Mater. Sci*., 1996, **6**, 15.

[4] G. Kresse, D. Joubert, *Phys. Rev. B*., 1999, **59**, 1758.

[5] P. E. Blöchl, *Phys. Rev. B*., 1994, **50**, 17953.

[6] J. P. Perdew, A. Ruzsinszky, G. I. Csonka, O. A. Vydrov, G. E. Scuseria, L. A. Con-stantin, X. Zhou, K. Burke, *Phys. Rev. Lett*., 2008, **100**, 136406.

[7] J. Heyd, G. E. Scuseria, *J. Chem. Phys*., 2003, **118**, 8207.

[8] A. V. Krukau, O. A. Vydrov, A. F. Izmaylov, G. E. Scuseria, *J. Chem. Phys*., 2006, **125**, 224106

[9] N. Marzari, D. Vanderbilt, *Phys. Rev. B*., 1997, **56**, 12847.

[10] I. Souza, N. Marzari, D. Vanderbilt, *Phys. Rev. B*., 2002, **65**, 1.

[11] G. Pizzi, V. Vitale, R. Arita, S. Blügel, F. Freimuth, G. Géranton, M. Gibertini, D. Gresch, C. Johnson, T. Koretsune et al., *J. Phys.: Condens. Matter.*, 2020, **32**, 165902.

[12] G. Henkelman, B. P. Uberuaga, H. Jónsson, *J. Chem. Phys*., 2000, **113**, 9901

[13] K. Momma, F. Izumi, *J. Appl. Cryst*. 2011, **44**, 1272.